Mathematical Modelling and Dynamics Analysis of Flat Multirotor Configurations

DENIS KOTARSKI, Department of Mechanical Engineering,
Karlovac University of Applied Sciences, J.J. Strossmayera 9, Karlovac, CROATIA,
denis.kotarski@vuka.hr
MATIJA PILJEK, Nanobit, Slovenska Street, Zagreb, CROATIA,
matija.piljek@nanobit.co
MARINA TEVČIĆ and VEDRAN VYROUBAL, Department of Mechanical Engineering,
Karlovac University of Applied Sciences, J.J. Strossmayera 9, Karlovac, CROATIA,
{marina.tevcic, vedran.vyroubal}@vuka.hr

Abstract: - Multirotor Unmanned Aerial Vehicles (UAV) are widely used in many applications such as surveillance, inspection operations and disaster site observations. There are various multirotor configurations which depend on the tasks requirements. In our case study, we investigated design considerations for a micro indoor multirotor. It consists of a frame, propulsion, sensors for indoor flight and open source autopilot which is suitable for control algorithm implementation. A full nonlinear mathematical model, which is divided into rigid body dynamics and control allocation scheme (CAS), is described. In this paper, a CAS matrix for flat multirotor configurations (FMRC) is derived which enable analysis of different multirotor properties such as agility, payload, power consumption, endurance and other. The series of measurements were conducted to present propulsion efficiency and to obtain aerodynamic coefficients. Various FMRC were analyzed through a series of open loop simulations. Results show that single FMRC have a much higher efficiency of coaxial FMRC while maintaining extreme agility.

Key-Words: - Multirotor UAV, 6 DOF, rigid body, CAS matrix, FMRC

1 Introduction

Multirotor UAVs can be potentially used for disaster site monitoring or search and rescue missions. Multirotors are autonomous or remotely piloted rotary-wing UAVs with fixed pitch propellers, typically small in size with extreme agility and maneuverability. They have the ability to carry out vertical take-off and landing (VTOL), as well as stationary and low-speed flight.

Multirotors have 6 DOF (degrees of freedom), the only moving parts are propellers with constant pitch connected to the rotor axis. It is assumed that the multirotor frame is symmetrical and rigid. Rotors angular velocities are only variables that have a direct impact on the multirotor dynamics. Multirotors are represented as highly nonlinear, multivariable and inherently unstable systems.

Multirotor UAVs configurations can be classified as FMRC and NFMRC (non-flat multirotor configuration). FMRC share properties of underactuated and strongly coupled systems. Various control units have built-in CAS matrix for conventional FMRC (quadrotor, hexarotor, octarotor, Y6 rotor, X8 rotor). The most common and by far the most popular FMRC is quadrotor which has four rotors [1, 2]. It is often used as an experimental platform for evaluation of complex control algorithms [3, 4].

Development and design of multirotors are considerably constrained by their size, weight and power consumption [5]. For proper selection of multirotor design according to the task requirements, it is necessary to obtain propulsion physical parameters [6]. Series of experiments were conducted in [7, 8] to evaluate the efficiency of coaxial propulsion. Some papers [9, 10] examine the influence of propulsion configuration and geometric arrangement on a system efficiency to achieve an increase in thrust for a limited body size.

In this paper, CAS matrix for FMRC is derived which enable dynamics analysis for the generic design of aircraft. It describes a mapping of the rotor angular velocities to a control vector. In our case study, we examined multirotor intended for the indoor flight which consists of sensors for an indoor flight that are compatible with an open source control unit (autopilot). Experimental measurements were conducted on components whose selection is based on the proposed case study.

2 Multirotor UAV Dynamic Model

The mathematical model describes aircraft dynamics with the respect to the input values and external influences. Multirotor dynamics is directly dependent on angular velocities of the propellers. Kinematics is described with two Cartesian coordinate systems as shown in Fig. 1.

Earth fixed frame (E-frame, $\mathcal{F}^E$) is the inertial right-handed coordinate system where positive direction of Z axis is in the direction normal to the earth ground level. Multirotor position $\boldsymbol{\xi} = [X \quad Y \quad Z]^{\mathrm{T}}$ and orientation $\boldsymbol{\eta} = [\phi \quad \theta \quad \psi]^{\mathrm{T}}$ are defined in $\mathcal{F}^E$. Roll-pitch-yaw convention order is applied.

Body fixed frame (B-frame, $\mathcal{F}^B$) is fixed on multirotor body and it is also right-handed coordinate system. Assumption is that the origin of $\mathcal{F}^B$ coincides with the multirotor center of gravity (COG) and that the principal inertia axes of multirotor body coincides with the $\mathcal{F}^B$ coordinate axes. Linear velocities $\mathbf{v}^{\mathrm{B}}$, angular velocities $\boldsymbol{\omega}^{\mathrm{B}}$, forces $\mathbf{F}$ and torques $\mathbf{T}$ are defined in $\mathcal{F}^B$

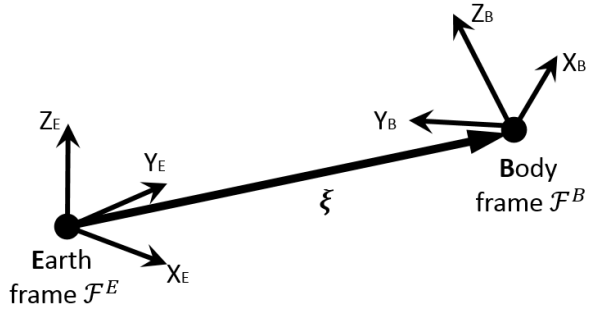

Figure 1. Multirotor UAV coordinate systems.

2.1 Multirotor UAV Kinematics

Multirotor UAV has 6 DOF. It is assumed that the multirotor frame is symmetrical and rigid. Kinematics of a rigid body with 6 DOF is given with:

$$\begin{bmatrix} \dot{\boldsymbol{\xi}} \\ \dot{\boldsymbol{\eta}} \end{bmatrix} = \begin{bmatrix} \mathbf{R} & \mathbf{0}_{3\times3} \\ \mathbf{0}_{3\times3} & \boldsymbol{\Omega}_{\boldsymbol{B}} \end{bmatrix} \begin{bmatrix} \mathbf{v}^{\mathbf{B}} \\ \boldsymbol{\omega}^{\mathbf{B}} \end{bmatrix} \tag{1}$$

where $\dot{\boldsymbol{\xi}}$ is the linear and $\dot{\boldsymbol{\eta}}$ is the angular velocity vector in $\mathcal{F}^E$. $\mathbf{R}$ is the rotation matrix which maps linear velocity vector from $\mathcal{F}^B$ to $\mathcal{F}^E$. It is given by

$$\mathbf{R} = \mathbf{R}(\psi, Z)\mathbf{R}(\theta, Y)\mathbf{R}(\phi, X) \tag{2}$$

where $\mathbf{R}(\psi, Z)$ denote the 3x3 fundamental rotational matrix around the Z axes and it is given by

$$\mathbf{R}(\psi, Z) = \begin{bmatrix} c_\psi & -s_\psi & 0 \\ s_\psi & c_\psi & 0 \\ 0 & 0 & 1 \end{bmatrix} \tag{3}$$

where $c_i = \cos(i)$, $s_j = \sin(j)$.
$\mathbf{R}(\theta, Y)$ is the rotational matrix around the Y axes

$$\mathbf{R}(\theta, Y) = \begin{bmatrix} c_\theta & 0 & s_\theta \\ 0 & 1 & 0 \\ -s_\theta & 0 & c_\theta \end{bmatrix} \tag{4}$$

$\mathbf{R}(\phi, X)$ is the rotational matrix around the X axes

$$\mathbf{R}(\phi, X) = \begin{bmatrix} 1 & 0 & 0 \\ 0 & c_\phi & -s_\phi \\ 0 & s_\phi & c_\phi \end{bmatrix} \tag{5}$$

Matrix $\boldsymbol{\Omega}_{\boldsymbol{B}}$ is the transformation matrix that transfers angular velocities from $\mathcal{F}^B$ to $\mathcal{F}^E$. It is given by

$$\boldsymbol{\Omega}_{\boldsymbol{B}} = \begin{bmatrix} 1 & s_\phi t_\theta & c_\phi t_\theta \\ 0 & c_\phi & -s_\phi \\ 0 & s_\phi / c_\theta & c_\phi / c_\theta \end{bmatrix} \tag{6}$$

where $t_i = \tan(i)$. Since the multirotor attitude being close to hovering state, $\boldsymbol{\Omega}_{\boldsymbol{B}}$ is close to the identity matrix, making the angular acceleration equations the same in $\mathcal{F}^E$ and $\mathcal{F}^B$.

2.2 Rigid Body Dynamics

Multirotor dynamics is described by multivariable and highly non-linear model. It consists of six-second order differential equations that were derived by using the Newton-Euler method [11]. The rigid body takes into consideration the mass m and the body inertia $\mathbf{I}$. It is divided into rigid body linear dynamics (7) and angular dynamics (8).

$$m\dot{\mathbf{v}}^{\mathrm{B}} + \boldsymbol{\omega}^{\mathbf{B}} \times (m\mathbf{v}^{\mathrm{B}}) = \mathbf{F} \tag{7}$$

$$\mathbf{I}\dot{\boldsymbol{\omega}}^{\mathrm{B}} + \boldsymbol{\omega}^{\mathbf{B}} \times (\mathbf{I}\boldsymbol{\omega}^{\mathrm{B}}) = \mathbf{T} \tag{8}$$

By applying the assumption that the multirotor frame has symmetrical structure inertia matrix becomes the diagonal matrix.

Force vector $\mathbf{F} = [F_X \quad F_Y \quad F_Z]^{\mathrm{T}}$ and the torque vector $\mathbf{T} = [T_\phi \quad T_\theta \quad T_\psi]^{\mathrm{T}}$ are defined with the respect to the $\mathcal{F}^B$. Generalized force vector $\boldsymbol{\Lambda} = [\mathbf{F} \quad \mathbf{T}]^{\mathrm{T}}$ can be divided into four components: gravitational vector $\mathbf{g}_{\mathrm{B}}(\boldsymbol{\xi})$, gyroscopic torque vector $\mathbf{o}_{\mathrm{B}}(\mathbf{v})\boldsymbol{\Omega}$, disturbance vector $\mathbf{d}$ and control vector $\mathbf{u}_{\mathrm{B}}$.

$$\mathbf{\Lambda} = \mathbf{g}_{\mathrm{B}}(\boldsymbol{\xi}) + \mathbf{o}_{\mathrm{B}}(\boldsymbol{\nu})\boldsymbol{\Omega} + \mathbf{d} + \mathbf{u}_{\mathrm{B}} \tag{9}$$

Gyroscopic torque vector introduces the gyroscopic effect to the model. It manifests itself in a form of a rotation around an unwanted axis, which is perpendicular to the axis of the rotor and the axis around which the wanted rotation is being achieved.

$$\mathbf{o}_{\mathrm{B}}(\boldsymbol{\nu})\boldsymbol{\omega} = \begin{bmatrix} \mathbf{0}_{3\times 1} \\ -\sum_{k=1}^{4} J_{TP}\,(\boldsymbol{\omega}^{\mathrm{B}} \times \mathbf{e}_3)(-1)^k \omega_k \end{bmatrix} \tag{10}$$

Gyroscopic torque vector has a little effect on the rigid body dynamics so it is often neglected.

Control vector $\mathbf{u}_{\mathrm{B}}(\boldsymbol{\omega})$ is represented by the product of CAS matrix $\mathbf{\Gamma}_{\mathrm{B}}$ and the vector of the propeller squared angular velocities $\boldsymbol{\Omega} = [{\omega_1}^2\ {\omega_2}^2\ \ldots\ {\omega_N}^2]^{\mathrm{T}}$.

$$\mathbf{u}_{\mathrm{B}} = \mathbf{\Gamma}_{\mathrm{B}}\boldsymbol{\Omega} \tag{11}$$

3 Force/Torque Mapping for FMRC

Based on the geometric arrangement of FMRC, the CAS matrix can be derived. At first, it is necessary to provide kinematic analysis of the connection between force/torque actuation and propulsion configuration.

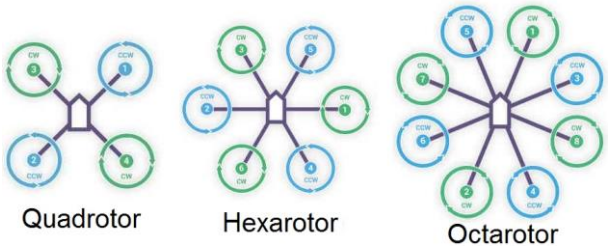

Figure 2. FMRC with single propulsion (PixHawk™ motor layout) [12].

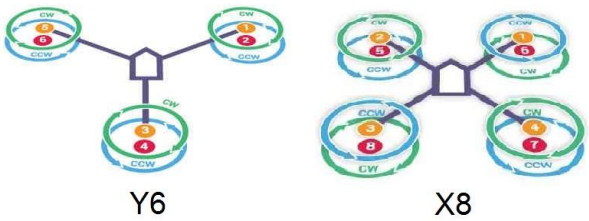

Figure 3. FMRC with coaxial propulsion (PixHawk™ motor layout) [12].

Multirotor configuration consists of an arbitrary number of rotors (N). Each rotor propeller generates an aerodynamic force which consists of thrust force and drag moment.

Rotor position $\boldsymbol{\xi}_{\mathrm{R}i}$ is defined as

$$\boldsymbol{\xi}_{\mathrm{R}i} = \begin{bmatrix} \cos\chi_i \\ \sin\chi_i \\ 0 \end{bmatrix} \cdot l \tag{12}$$

where χ_i is the i-th rotor angle around the Z_B axis and l is the distance from rotor to COG. Rotor orientation vector for ith rotor is a unit vector $\mathbf{e}_3$, since it is parallel with Z_B axis.

3.1 Propulsion forces and torques

After geometry analysis of FMRC is presented, forces and torques that are generated by propeller rotation can be derived.

Each propeller generates force vector which can be calculated by the following equation

$$\mathbf{f}_i = (b\mathbf{e}_3){\omega_i}^2 \tag{13}$$

where ω_i is angular speed of the ith rotor, and b is the thrust coefficient Ns^2.

Each propeller also generates torque vector which can be calculated by the following equation

$$\boldsymbol{\tau}_i = (b\boldsymbol{\xi}_{\mathrm{R}i} \times \mathbf{e}_3 + P_i d\mathbf{e}_3){\omega_i}^2 \tag{14}$$

where d is the drag coefficient Nms^2, and P_i is the signum of ith propeller rotation. Clockwise (CW) rotation is positive and counter clockwise (CCW) is negative.

$$P_i = sign(\omega_i) \tag{15}$$

From the static thrust test, constants b and d can be obtained. They depend on the propeller radius, thrust and power factor, and air density.

3.2 CAS matrix

Control allocation scheme is a 6xN matrix where 6 represent three forces and three torques while N represents a number of rotors. It is derived from equations (13) and (14).

$$\mathbf{\Gamma}_{\mathrm{B}} = \begin{bmatrix} b\mathbf{e}_3 & \ldots & b\mathbf{e}_3 \\ b\mathbf{S}(\boldsymbol{\xi}_{\mathrm{R}_1})\mathbf{e}_3 + P_1 d\mathbf{e}_3 & \ldots & b\mathbf{S}(\boldsymbol{\xi}_{\mathrm{R}_N})\mathbf{e}_3 + P_N d\mathbf{e}_3 \end{bmatrix} \tag{16}$$

From (16) it can be seen that FMRC provides only four independent control variables because CAS matrix has a rank no greater than four. Regardless of the number of actuators, FMRC shares inherent underactuated condition. Equation 17 shows CAS

matrix for hexarotor with rotors geometric arrangement according to Figure 2b.

$$\boldsymbol{\Gamma}_{\mathrm{B}} = \begin{bmatrix} 0 & 0 & 0 & 0 & 0 & 0 \\ 0 & 0 & 0 & 0 & 0 & 0 \\ b & b & b & b & b & b \\ bl & bl & \frac{1}{2}bl & -\frac{1}{2}bl & -\frac{1}{2}bl & \frac{1}{2}bl \\ 0 & 0 & -\frac{\sqrt{3}}{2}bl & \frac{\sqrt{3}}{2}bl & -\frac{\sqrt{3}}{2}bl & \frac{\sqrt{3}}{2}bl \\ d & -d & d & -d & -d & d \end{bmatrix} \quad (17)$$

3.3 Control vector

The rotor system force vector $\mathbf{f} = [f_X \quad f_Y \quad f_Z]^{\mathrm{T}}$ is defined as

$$\mathbf{f} = \sum_{i=1}^{N} \mathbf{f}_i \quad (18)$$

The rotor system torque vector $\boldsymbol{\tau} = [\tau_\phi \quad \tau_\theta \quad \tau_\psi]^{\mathrm{T}}$ is defined as

$$\boldsymbol{\tau} = \sum_{i=1}^{N} \boldsymbol{\tau}_i \quad (19)$$

Considering aerodynamic effects, it follows that forces and moments are proportional to the squared angular velocities of the propellers. Control vector $\mathbf{u}_{\mathrm{B}}(\boldsymbol{\omega}) = [\mathbf{f} \quad \boldsymbol{\tau}]^{\mathrm{T}}$ is represented by the product of control allocation scheme $\boldsymbol{\Gamma}_{\mathrm{B}}$ and the vector of squared propeller angular velocities $\boldsymbol{\Omega}$. Control vector is input in the rigid body dynamic model.

For the control design and implementation on an aircraft prototype, it is necessary to calculate the angular velocity for each individual propulsion.

$$\boldsymbol{\Omega} = \boldsymbol{\Gamma}_{\mathrm{B}}{}^{-1}\mathbf{u}_{\mathrm{B}} \quad (20)$$

4 Propulsion analysis

For the purpose of our case study, propulsion configurations with 4” and 5” propellers were examined.

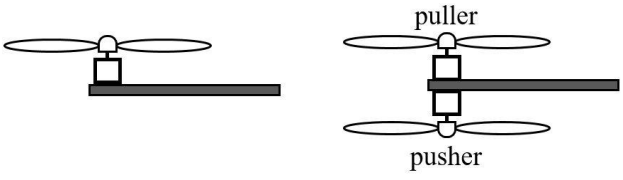

Figure 4. Single propulsion configuration a), coaxial propulsion configuration b).

Table 1. Examined propulsion configurations.

Propulsion configuration	Puller propeller	Pusher propeller
Single	4040_2	-
	4045_2_BN	-
	4045_3	-
	4045_3_BN	-
Coaxial	4045_2_BN	4045_2_BN
Single	5030_2	-
	5030_3	-
	5040_2	-
	5040_3	-
	5040_4	-
	5040_6	-
	5046_2_BN	-
	5050_3_BN	-
Coaxial	5030_2	5030_2
	5040_2	5040_2
	5030_2	5040_2

Where label xxyy_w_BN stands for xx – diameter, yy – pitch, w – number of blades, BN – bull nose geometric feature of propeller design. The experimental measurements were conducted to obtain dependencies of aerodynamic forces, the angular velocity of the rotor and power consumption in relation to a control signal.

4.1 Efficiency

Propulsion efficiency is crucial for proper selection of propulsion configuration. It is given by the ratio of the thrust and consumed power.

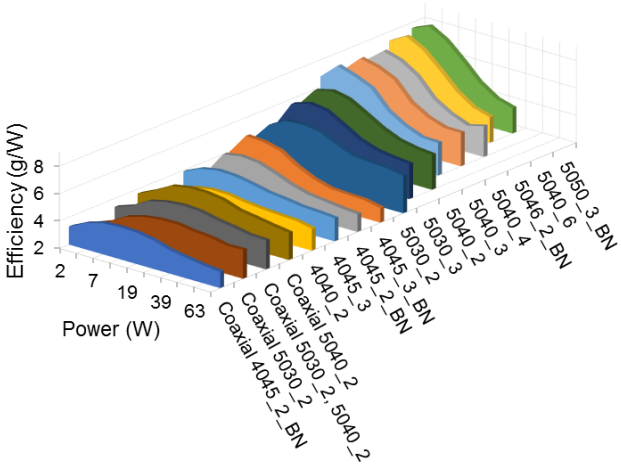

Figure 5. Propulsion efficiency.

Measurements (Figure 5) show that the increase of propeller diameter in general results in better efficiency. Higher pitch or number of blades results

in an additional thrust. Coaxial propulsion configuration has lower efficiency than single.

4.2 Aerodynamic force coefficients

For dynamics simulation, the thrust force (Figure 6) and drag moment coefficient have been estimated from the experimental measurements.

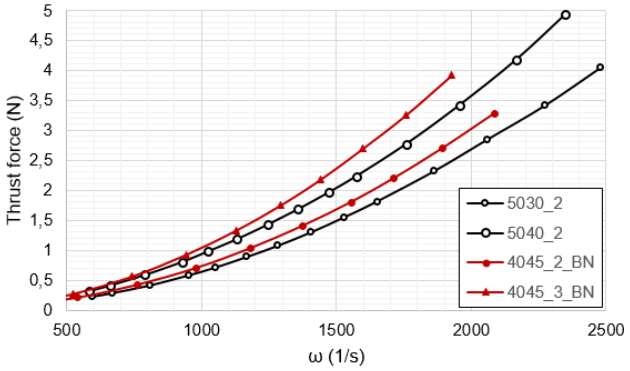

Figure 6. Thrust force as a function of the angular velocity.

5 Simulation results

FMRC (Figure 2 and 3) were analyzed through a series of open loop simulations. Hovering autonomy for generic designed aircraft is shown in Table 2 and Table 3.

Table 2. Hoovering autonomy for single FMRC

Single FMRC	**Hoovering autonomy (min)**		
Puller	X4	H6	O8
4045_2_BN	11	10.5	10.8
4045_3_BN	10.6	10.5	11.3
5030_2	16.2	15	14.6
5040_2	15.5	15.7	15.5

Table 3. Hoovering autonomy for coaxial FMRC

Coaxial FMRC		**Hoovering autonomy (min)**	
Puller	Pusher	Y6	X8
4045_2_BN	4045_2_BN	6.7	6
5030_2	5030_2	-	7.4
5030_2	5040_2	9	7.9
5040_2	5040_2	9	8.1

Tables 2 and 3 shows that the FMRC with single propulsion has a much higher hovering autonomy than FMRC with coaxial propulsion. Also, propulsion efficiency increases with increasing propeller diameter. Coaxial propulsion configuration will be further investigated for larger sized aircraft.

For dynamic analysis, physical parameters were obtained from generic design and propulsion data.

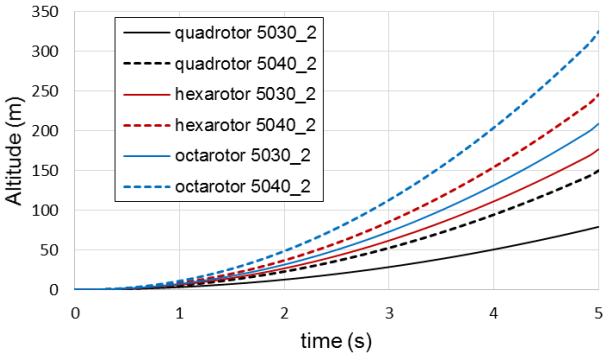

Figure 7. Ideal altitude (Z) at maximum thrust.

From Figure 7, it can be seen that the proposed configurations have extreme vertical acceleration, therefore, could be used for different tasks.

6 Conclusion

In this paper, CAS matrix for FMRC is derived which describes a mapping of the rotor angular velocities to a control vector. The derived CAS matrix has rank no greater than four, therefore FMRC has four independent control variables. It follows that FMRC are underactuated and strongly coupled systems regardless of the number of actuators. This property has a significant influence on multirotor dynamics and control design.

Through series of experiments, it is demonstrated that single propulsion has much greater efficiency than coaxial. By increasing the propeller diameter result in increasing the propulsion efficiency, out of which follows an increase in aircraft dimensions. Furthermore, larger diameter reduces the efficiency difference between single and coaxial propulsion. The described mathematical model allows a series of open loop simulations which enable FMRC selection based on physical parameters and aircraft propulsion.

Future work will be focused on the control design and a development of Indoor FMRC which will be used for implementation of the tracking control algorithms.

References:

[1] S. Bouabdallah, P. Murrieri and R. Siegwart, Design and Control of an Indoor Micro Quadrotor, *Robotics and Automation, 2004. Proceedings. ICRA'04. 2004 IEEE International*

Conference on Robotics and Automation, vol 5, 4393-4398, 2004.

[2] P. Pounds, R. Mahony, P. Hynes and J. Roberts, Design of a Four-Rotor Aerial Robot, *Proceedings. 2002 Australasian Conference on Robotics and Automation (ACRA 2002)*, 145-150, 2002.

[3] D. Cabecinhas, R. Cunha and C. Silvestre, A Globally Stabilizing Path Following Controller for Rotorcraft With Wind Disturbance Rejection, *IEEE TRANSACTIONS ON CONTROL SYSTEMS TECHNOLOGY*, vol 23(2), 708-714, 2015.

[4] L. Wang and J. Su, Robust Disturbance Rejection Control for Attitude Tracking of an Aircraft, *IEEE TRANSACTIONS ON CONTROL SYSTEMS TECHNOLOGY*, vol 23(6), 2015.

[5] Y. Mulgaonkar, M. Whitzer, B. Morgan, C. M. Kroninger, A. M. Harrington and V. Kumar, Power and Weight Considerations in Small, Agile, Quadrotors, *Proceedings of SPIE - The International Society for Optical Engineering*, vol 9083, 90831Q-1-90831Q-16, 2014.

[6] S. D. Prior and J. C. Bell, Empirical Measurements of Small Unmanned Aerial Vehicle Co-Axial Rotor Systems, *Journal of Science and Innovation*, vol 1, No 1, 1-18, 2011.

[7] C. M. Simoes, Optimizing a Coaxial Propulsion System to a Quadcopter, https://fenix.tecnico.ulisboa.pt/downloadFile/563345090412782/Resumo.pdf

[8] A. Bondyra, S. Gardecki, P. Gasior and W. Giernacki, Performance of Coaxial Propulsion in Design of Multi-rotor UAVs, *Challenges in Automation, Robotics and Measurement Techniques, vol 440, Advances in Intelligent Systems and Computin*g pp 523-531, 2016.

[9] H. Otsuka and K. Nagatani, Thrust Loss Saving Design of Overlapping Rotor Arrangement on Small Multirotor Unmanned Aerial Vehicles, 2016 *IEEE International Conference on Robotics and Automation (ICRA)*, 3242-3248, 2016.

[10] B. Theys, G. Dimitriadis, P. Hendrick and J. De Schutter, Influence of propeller configuration on propulsion system efficiency of multi-rotor Unmanned Aerial Vehicles, 2016 *International Conference on Unmanned Aircraft Systems (ICUAS)*, 195-201, 2016.

[11] T. Bresciani, Identification and control of a quadrotor helicopter, Department of Automatic Control, Lund University, 2008.

[12] http://ardupilot.org/copter/docs/connect-escs-and-motors.html